Desalination and Water Treatment
www.deswater.com

doi: 10.5004/dwt.2019.23181

137 (2019) 114–124
January

Core/shell magnetic nanoparticles of $Fe_3O_4/Mn_xZn_yFe_{3-x-y}O_4$ for phosphate adsorption from water: effects of adsorbent composition using response surface methodology

Masome Mirzapour, Faranak Akhlaghian*

Department of Chemical Engineering, Faculty of Engineering, University of Kurdistan, Sanandaj, Iran, Tel. +98 87 33664600; Fax: +98 87 33668513; emails: akhlaghianfk@gmail.com (F. Akhlaghian), m.chemengineering@gmail.com (M. Mirzapour)

Received 28 January 2018; Accepted 24 September 2018

ABSTRACT

The effects of the concentrations of shell constituent solutions and core mass of $Fe_3O_4/Mn_xZn_yFe_{3-x-y}O_4$ on phosphate adsorption were investigated using response surface methodology. An empirical mathematical model was developed which relates the response, that is, phosphate adsorption from water to the independent variables, that is, concentrations of Mn^{2+} and Zn^{2+} solutions (shell constituent solutions), and core (Fe_3O_4) mass using Design Expert software (version 7). *F* and *p*-values showed the significance of the model. The adsorbent was synthesized based on one of the optimal points suggested by the software and characterized by inductively coupled plasma spectroscopy, X-ray crystallography, X-ray photoelectron spectroscopy, transmission electron microscopy, scanning electron microscopy, and vibrating sample magnetometery methods. The experimental data corresponded to the Langmuir adsorption model. Statistical analysis indicated that the quadratic term of Fe_3O_4 mass had the highest effect on the phosphate adsorption yield. Also, the interaction term between the Fe_3O_4 mass and the Mn^{2+} solution concentration and linear term of Zn^{2+} solution had significant effects on phosphate adsorption. The results confirmed interaction between variables. Accordingly, the adsorbent yield for phosphate removal is a strong function of $Fe_3O_4/Mn_xZn_yFe_{3-x-y}O_4$ composition.

Keywords: Phosphate adsorption; Response surface methodology; Wastewater treatment; Core/shell; Magnetic nanoparticles

1. Introduction

Phosphate is one of the most important macronutrients for the growth of humans and other living beings. Phosphate enters water sources via agricultural, industrial, and domestic activities [1–3]. Excessive phosphate in water causes the overgrowth of algae and cyanobacterial leading to eutrophication phenomena [4]. Eutrophication depletes dissolved oxygen of water, which endangers the lives of aquatic species and can also disturb the food chain [5,6]. Concerns about water quality degradation due to eutrophication have brought about a lot of research studies to be conducted on phosphate removal from water and wastewater [7–10].

Various technologies have been applied for removal of phosphate from water including chemical, physical, ion exchange, membrane, and biological methods [1,5,11]. Chemical methods produce high amounts of sludge. Biological methods can remove high percentage of phosphate but additional treatment stages are always required [5]. Membrane processes have high maintenance costs and are prone to degradation, thus they are not economically efficient [12]. Among these techniques, adsorption has attained attraction due to advantages such as operational simplicity, cost effectiveness, and eliminating the posttreatment stages [1,5].

High specific surface area and selectivity are desirable characteristics for adsorbents. Nanotechnology paves the way for preparing suitable adsorbents. Nanoparticles have a wide range of applications in fields such as catalysis, medicine, sensors, and information technology [3,5,13].

* Corresponding author.

Magnetic nanoparticles have been extensively used in water remediation [14,15].

Various types of adsorbents have been investigated for phosphate removal such as fly ash, red mud, activated carbon, magnetite, metal oxides, and metal hydroxides [1,9]. One of the most common adsorbents is magnetite (Fe_3O_4). Magnetite is ferrimagnetic. Its nanosized particles are easy to prepare, have high surface area, and are easily separable from water due to their magnetic property [16–18]. Magnetite is susceptible to oxidation and conversion to hematite (Fe_2O_3). Covering magnetite with other stable nanoparticles can prevent it from oxidation and enhance its yield for phosphate adsorption [19,20]. Zhang et al. [21] used a coprecipitation process to synthesize Fe-Mn binary oxide adsorbent to remove phosphate from water. The magnetic Fe-Zr binary oxide was synthesized and used for phosphate adsorption from water by Long et al. [22]. They found out that easy separation from water and efficient reusability were the advantages of the magnetic Fe-Zr adsorbent [22]. Yang et al. [19] showed that the uptake rate of phosphate in water by La-EDTA-Fe_3O_4 was 3–1,000 times more than EDTA-Fe_3O_4. Yoon et al. [23] investigated the phosphate removal by magnetic iron oxide nanoparticles. Three different magnetic core/shell Fe_3O_4/LDH (layer double hydroxide) were applied by Yan et al. for phosphate removal. The maximum phosphate removal was in the order: Fe_3O_4/Zn-Al-LDH > Fe_3O_4/Mg-Al-LDH > Fe_3O_4/Ni-Al-LDH [9]. Lai et al. [24] achieved high adsorption by first covering Fe_3O_4 by SiO_2 layer for protecting it from oxidation and then doping with lanthanum.

In this work, novel magnetic nanoparticles of $Mn_xZn_yFe_{3-x-y}O_4$ coated Fe_3O_4 were synthesized for phosphate adsorption. $Mn_xZn_yFe_{3-x-y}O_4$ coating results in magnetic material which can improve the phosphate adsorption on adsorbent without lessening its magnetic property. The effects of the shell constituents (Mn, Zn, and Fe) and core (Fe_3O_4) on phosphate removal adsorption were investigated. Response surface methodology (RSM) was used for the experimental design.

2. Materials and methods

2.1. Materials

Ferric nitrate ($Fe(NO_3)_3{\cdot}9H_2O$), ferrous sulfate ($FeSO_4{\cdot}7H_2O$), trisodium citrate ($Na_3C_6H_5O_7{\cdot}2H_2O$), manganese chloride ($MnCl_2{\cdot}4H_2O$), zinc sulfate ($ZnSO_4{\cdot}7H_2O$), potassium dihydrogen phosphate (KH_2PO_4), sodium hydroxide (NaOH), aqueous ammonia solution ($NH_3{\cdot}H_2O$), acetone (C_3H_6O), and hydrazine hydrate ($N_2H_4{\cdot}H_2O$) were used. All chemicals were of analytical grade and purchased from Merck Company (Germany). Industrial grade of N_2 gas was purchased. In all experiments, deionized water was used.

2.2. Synthesis of Fe_3O_4 nanoparticles

The synthesis of Fe_3O_4 was carried out by a coprecipitation method. Solutions of $FeSO_4$ (0.5 M) and $Fe(NO_3)_3$ (0.5 M) were prepared and mixed with a molar ratio of 1.75:1 under the protection of N_2 gas. After adding 10 mL of aqueous ammonia, some hydrazine hydrate was dropped into the mixture until the pH of the solution reached 9. Then, this solution was stirred at 60°C for 30 min. Finally, the black precipitate was collected by a magnet and washed several times with deionized water until the pH decreased to 7 [25,26].

2.3. Modification

Fe_3O_4 nanoparticles (1 g) were dispersed in a 100 mL trisodium citrate (0.1 M) and exposed to ultrasonic irradiation for 30 min. The suspension was stirred at 60°C for 12 h under the protection of N_2 gas. The precipitate was separated from the suspension with a magnet and washed several times with acetone to remove the remainder of sodium citrate. Coating of Fe_3O_4 nanoparticles with citrate ions prevented the agglomeration of Fe_3O_4 nanoparticles and negatively charged its surface by carboxylic groups [25,26].

2.4. Synthesis of $Fe_3O_4/Mn_xZn_yFe_{3-x-y}O_4$

The mixture of the solution of $MnCl_2$ (50 mL, X_1 molar), $ZnSO_4$ (50 mL, X_2 molar), and $Fe(NO_3)_3$ (50 mL, 3-X_1-X_2 molar) was prepared under protection of N_2 gas. The mixture was stirred and heated gradually to 90°C. Then, the modified magnetic nanoparticles of Fe_3O_4 (X_3 g) were added to the prepared solution and stirred for 30 min in N_2 atmosphere. Experimental design determined the amounts of X_1, X_2, and X_3. NaOH solution (50 mL, 0.1 molar) was added to the mixture. Then the mixture was stirred at 90°C for 1 h in N_2 atmosphere. Finally, the precipitate was collected and separated from the solution by a magnet and washed several times by deionized water until the effluent solution reached neutral pH. The precipitate was dried at 100°C for 12 h in an oven. At this stage, $Mn_xZn_yFe_{3-x-y}O_4$ nanoparticles covered the surface of modified Fe_3O_4 nanoparticles [26].

2.5. Batch experiments of phosphate adsorption

Core/shell magnetic nanoparticles of $Fe_3O_4/Mn_xZn_yFe_{3-x-y}O_4$ were used as adsorbent. 1 g of $Fe_3O_4/Mn_xZn_yFe_{3-x-y}O_4$ adsorbent, and 200 mL of aqueous phosphate solution with the concentration of 200 mL and pH of 6–7 were mixed in a well-sealed flask and stirred for 3 h. Then, the adsorbent was separated magnetically from the mixture. The concentration of phosphate in the remnant solution was measured by molybdate blue method using UV-Vis spectrophotometer (TG 80+, UK) at the wavelength of 880 nm [27,28]. The removal of phosphate was measured by Eq. (1) as follows [19]:

$$\text{Phosphate removal}(\%) = \frac{C_i - C_f}{C_i} \times 100 \quad (1)$$

where C_i and C_f are the initial and final phosphate concentrations, respectively. Each experiment was triplicated and the average was reported.

2.6. Characterization

The X-ray diffraction (XRD) patterns were obtained by X'Pert MPD diffractometer (Philips, Netherland) using Co-K_α radiation. Morphological studies on the surface of the nanoparticles were carried out using field emission scanning electron microscope (FESEM) on 300 kV accelerated voltage

(TESCAN, Czech). The shape and size of the nanoparticles were determined by transmission electron microscope (TEM Philips CM 30, Netherland). The elemental analysis of the nanoparticles was obtained by inductively coupled plasma (ICP) optical emission spectroscopy 730-ES (Varian, USA). The magnetic property of the adsorbent was measured using a vibrating sample magnetometer (VSM) (Kavir Kashan, Iran). The X-ray photoelectron spectroscopy (XPS) was performed by a VG Microtech XR3E2 spectrometer with Al K_α (1,486 eV) radiation source.

2.7. Experimental design

RSM is a collection of mathematical and statistical approaches, which represents a functional relationship for the response of interest as a function of multiple variables and the interaction between them. Based on the complexity of the process, linear, quadratic, or cubic equations are required for modeling of the process [29]. D-optimal is a mathematical algorithm and can be combined with RSM to minimize the generalized variance of the predicted response [30]. In this work, D-optimal combined with RSM was utilized to optimize the formulation of $Fe_3O_4/Mn_xZn_yFe_{3-x-y}O_4$ for suitable removal of phosphate from water.

The adsorbent composition is related to the constituent solutions, so concentrations of $ZnSO_4$ solution (X_1 molar) and $MnCl_2$ solution (X_2 molar) and mass of modified Fe_3O_4 (X_3 g) were chosen as independent variables. They were introduced to Design Expert software (version 7) to assess their effects on phosphate removal and to prepare the optimal adsorbent. Ranges of the independent variables in three levels are shown in Table 1. It is necessary to mention that the concentration of the $Fe(NO_3)_3$ solution was changed in every experiment according to the equation of $[Fe(NO_3)_3] = 3\text{-}X_1\text{–}X_2$ with the aim of obtaining iron spinel structure [31]. Thus, the concentration of the $Fe(NO_3)_3$ solution was not introduced to the software as an independent variables and the layout of the 19 experiments which were generated by Design Expert are shown in Table 2. The coded variables are calculated according to Eq. (2) as follows:

$$x_i = \frac{X_i - X_{0,i}}{X_{\max,i} - X_{0,i}} \tag{2}$$

where x_i is the coded variable, X_i is the actual value of the variable, $X_{0,i}$ is the middle point of the variation range, and $X_{\max,i}$ is the highest value of variable i.

3. Results and discussions

3.1. Statistical analysis

The empirical model of the phosphate adsorption in terms of coded variables was developed by Design Expert (version 7) as follows:

$$\begin{aligned} R1(\text{Phosphate removal\%}) = {} & 77.34 + 18.09x_1 - 25.38x_2 + \\ & 12.68x_1x_2 - 10.39x_1x_3 - 21.65x_2x_3 - 24.63x_2^2 - 32.48x_3^2 + \\ & 6.51x_1x_2x_3 + 30.49x_1^2x_2 - 9.85x_1^2x_3 \end{aligned} \tag{3}$$

Table 1
Ranges and levels of the independent variables for D-optimal design

Variables	Ranges and levels		
	−1	0	+1
Concentration of $ZnSO_4$ solution (mol/L)	0.1	1.1	2.1
Concentration of $MnCl_2$ solution (mol/L)	0.1	0.45	0.8
Modified Fe_3O_4 (g)	0.5	2.25	4

Table 2
Matrix of the experiments and their reported responses

Run	X_1 (mol/L)[a]	X_2 (mol/L)[b]	X_3 (g)[c]	Yield of phosphate removal (%)	
				Experimental	Predicted
1	2.1	0.10	0.5	24.00	25.63
2	2.07	0.11	2.25	60.00	53.01
3	2.10	0.10	4.00	19.00	20.73
4	1.35	0.80	2.69	28.00	29.09
5	0.90	0.52	1.81	64.00	66.09
6	0.1	0.80	2.74	16.00	16.77
7	2.1	0.10	4.00	14.00	15.43
8	2.1	0.80	4.00	23.00	20.73
9	0.10	0.10	4.00	38.00	38.41
10	0.10	0.10	4.00	39.00	38.41
11	0.10	0.35	0.50	16.00	18.53
12	2.10	0.10	0.50	26.00	25.63
13	2.03	0.45	3.95	46.00	42.71
14	0.91	0.52	4.00	33.00	32.01
15	0.91	0.10	1.91	69.00	69.56
16	0.1	0.80	2.74	18.00	16.77
17	0.1	0.35	0.50	21.00	18.53
18	1.41	0.80	0.50	32.00	31.12
19	0.10	0.80	0.50	22.00	22.19

[a] Concentration of $ZnSO_4$solution
[b] Concentration of $MnCl_2$ solution
[c] Mass of modified Fe_3O_4

The response of the process is the phosphate removal percentage (%). x_1, x_2, and x_3 are coded variables corresponding to the $ZnSO_4$ and $MnCl_2$ solutions concentrations and mass of the modified Fe_3O_4, respectively.

The analysis of variance (ANOVA) results of the model are presented in Table 3. In statistical view, the significance of the model is determined by its Fisher and probability values [29]. The model is more significant with higher F-value and smaller p-value. According to the ANOVA table, F-value of 87.88 and p-value of 0.0001 indicate significance of the model at 99.99% confidence level [29].

Fig. 1 illustrates the experimental results versus the model predicted values. The points are located on the 45° line due to suitable values of R^2 and Adj R^2. The values of R^2 (0.9910) and Adj R^2 (0.9970) are close to unity which imply a good agreement between experimental and predicted model values. The adequate precision of the model (29.969)

Table 3
Analysis of variance for the phosphate removal model

Source	Sum of squares (SS)	Degree of freedom (df)	Mean square (MS)	*F*-value	*p*-value Prob > *F*
Model	5,032.19	10	5,032.19	87.88	<0.0001
x_1	1,513.75	1	1,513.75	264.36	<0.0001
x_2	1,958.86	1	1,958.86	184.92	<0.0001
x_1x_2	750.22	1	750.22	131.02	<0.0001
x_1x_3	392.40	1	392.40	68.53	<0.0001
x_2x_3	1,666.98	1	1,666.98	291.11	<0.0001
x_2^2	1,101.99	1	1,101.99	192.45	<0.0001
x_3^2	2,145.77	1	2,145.77	374.73	<0.0001
$x_1x_2x_3$	125.32	1	125.32	21.89	0.0016
$x_1^2x_2$	722.17	1	722.17	126.12	<0.0001
$x_1^2x_3$	419.22	1	419.22	73.21	<0.0001
Residual	45.81	8	5.73		
Lack of fit	20.81	3	6.94	1.39	0.3486
Pure error	25.00	5	5.00		

x_1: $ZnSO_4$ solution concentration (dimensionless); x_2: $MnCl_2$ solution concentration (dimensionless); x_3: mass of modified Fe_3O_4 (dimensionless); *R*-squared = 0.9910; Adj *R*-squared = 0.9970; Adequate precision = 29.969.

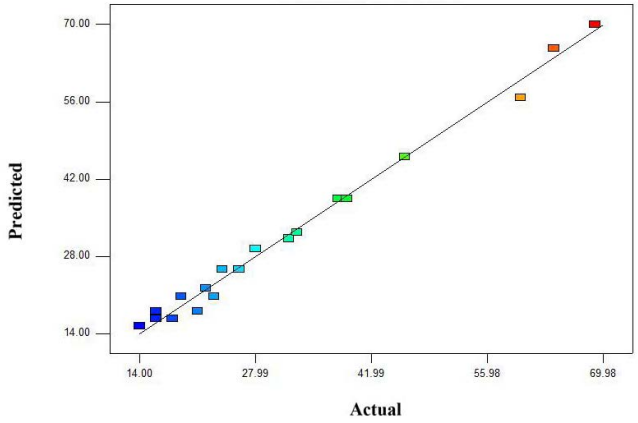

Fig. 1. Predicted versus experimental values.

is greater than 4 which shows that the model can be used to navigate the design space [32].

The *p*- and *F*-values are applied to determine the significance of different terms in the prediction of the response [33]. Terms with smaller *p*-value and larger *F*-values are more significant and have more effect on the response. In this model, the quadratic term of the modified Fe_3O_4 mass (x_3^2) had the largest effect on the phosphate removal at 99.99% confidence level due to its *p*-value (<0.0001) and the highest *F*-value (374.73). The interaction term between modified Fe_3O_4 mass and Mn^{2+} solution concentration (x_2x_3) with *F*-value of 291.11 and *p*-value <0.0001 at 99.99% confidence level affected the response. After these terms, linear term of Zn^{2+} solution concentration (x_1) and quadratic term of Mn^{2+} solution concentration (x_2^2) had significant effects on the response. The other term in significant orders is: x_2, x_1x_2, $x_1^2x_2$, $x_1^2x_3$, x_1x_3, $x_1x_2x_3$. In general, the significant order of independent variables on phosphate removal is: modified Fe_3O_4 mass (core), Mn^{2+} and Zn^{2+} solutions concentrations.

3.2. Effects of the variables on phosphate adsorption

Two-dimensional contours and three-dimensional diagrams for phosphate adsorption by $Mn_xZn_yFe_{3-x-y}O_4$ coated on Fe_3O_4 are illustrated in Fig. 2. An increase of the Zn^{2+} solution concentration from its lowest level 0.1–2.1 mol/L increased phosphate adsorption (Figs. 2(a) and (b)). For all values of the Zn^{2+} solution concentration, increasing Fe_3O_4 from 0.5 to 4 g first increased the phosphate removal yield but then decreased the phosphate adsorption. The magnetic dipole–dipole attractions among magnetic nanoparticles can also increase the tendency for aggregation [26]. It can be concluded that larger particles decreased the phosphate adsorption.

In all values of Fe_3O_4 (Figs. 2(c) and (d)) when Mn^{2+} concentration increased from 0.1 to 0.8 mol/L, an increasing decreasing trend in the phosphate adsorption was observed; hence, there were optimum values for Mn^{2+} concentration. Figs. 2(c) and (d) show that when Fe_3O_4 increased from 0.5 to 4 g, first the phosphate adsorption increased, then reaches to the maximum, and finally decreased. The aggregation of magnetic nanoparticles and reduction of the surface area can explain it [26].

Figs. 2(e) and (f) show phosphate adsorption at fixed Fe_3O_4 of 2.6 g. Inclined and curved contours show an interaction between Zn^{2+} and Mn^{2+} concentrations. At a constant Zn^{2+} concentration, phosphate adsorption first increased and then decreased when the Mn^{2+} concentration increased. Figs. 2(e) and (f) show that phosphate adsorption increased when Zn^{2+} concentration increased but an exception was observed at low Mn^{2+} concentration.

Figs. 3(a) and 3(b) show the effects of Fe^{3+} solution concentration (one of the shell constituent elements). Fig. 3(a) shows that at all values of Zn^{2+}, the adsorption first increased and then decreased when Fe^{3+} concentration increased. It is clear from Fig. 3(b) that at low and high Mn^{2+} concentrations, the trends of the phosphate adsorption are not the same.

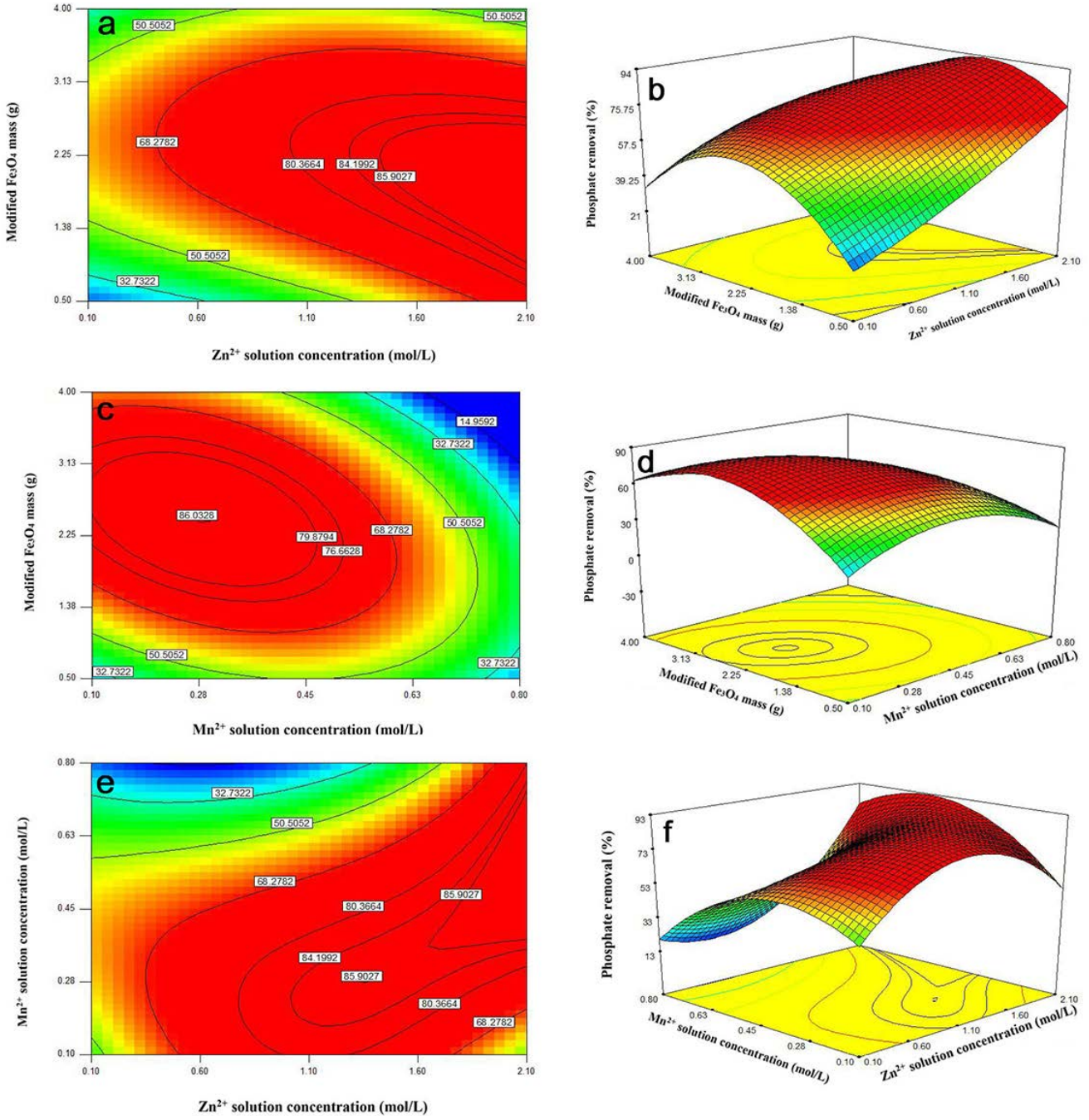

Fig. 2. Surface plots and contours show the effects of the independent variables on phosphate adsorption; (a) and (b) Mn^{2+} concentration is constant at 0.38 mol/L; (c) and (d) Zn^{2+} concentration is constant at 1.3 mol/L; (e) and (f) Fe_3O_4 mass is constant at 2.6 g.

At low Mn^{2+} concentration, when Fe^{3+} increased phosphate adsorption first increased and then decreased but at high Mn^{2+} concentrations, when Fe^{3+} increased phosphate adsorption first decreased and then increased.

Accordingly, the yield of core/shell adsorbent $Mn_xZn_yFe_{3-x-y}O_4$ coated on Fe_3O_4 is a strong function of Mn^{2+}, Zn^{2+}, Fe^{3+} solutions concentrations, Fe_3O_4 mass and their interactions. The interactions terms of x_2x_3, x_1x_2, $x_1^2x_2$, $x_1^2x_3$, x_1x_3, and $x_1x_2x_3$ of the empirical model affected the response. The high *F*-values and low *p*-values show statistically significant effects of the interactions terms on the response.

3.3. Optimization

The previous section shows that phosphate adsorption removal by the core/shell adsorbent was a strong function of the Fe_3O_4 mass (core) and shell constituent composition. Wrong selection of the composition concentrations can lead to a poor adsorbent, so it is necessary to optimize the synthesis.

Optimization was carried out by Design Expert software (version 7) to find the points of maximum phosphate adsorption; 30 points were suggested. One of these points

Table 4
Optimum experimental and predicted results

Optimum condition				Phosphate adsorption (%)	
Mn^{2+} solution concentration (mol/L)	Zn^{2+} solution concentration (mol/L)	Fe^{3+} solution concentration (mol/L)	Modified Fe_3O_4 mass (g)	Experimental	Predicted
0.49	0.6	1.91	2.17	59.48%	52.79%

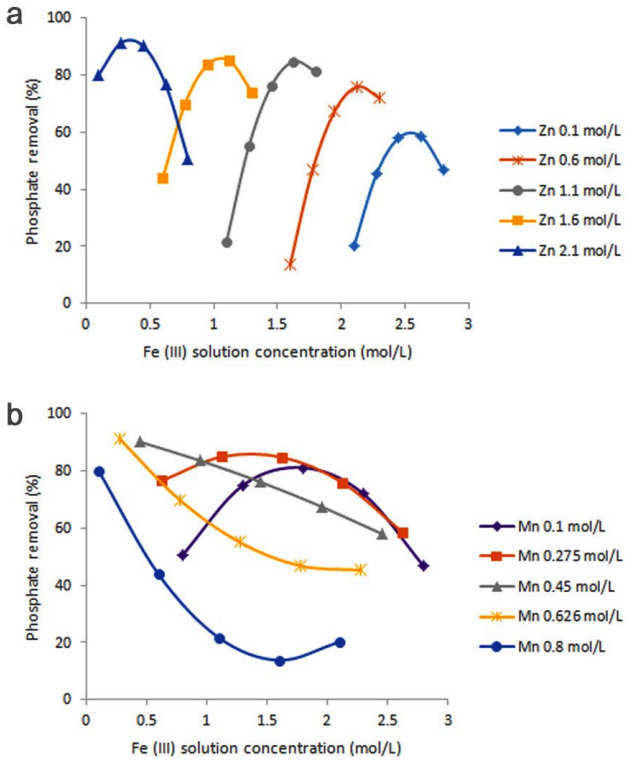

Fig. 3. Effect of Fe^{3+} solution concentration on phosphate removal; Fe_3O_4 mass is constant at 2.6 g; (a) Zn^{2+} solution concentration is constant at 1.3 mol/L; (b) Mn^{2+} solution concentration is constant at 0.38 mol/L.

was selected and validated by the experiment. The predicted adsorption was reliable by 6.69% difference with respective experimental result. Table 4 shows that 59.48% of phosphate adsorption was achieved by its respective Mn, Zn, and Fe concentration and Fe_3O_4 mass. This adsorbent was used for characterization.

3.4. Characterization

The shell was synthesized without core and analyzed by ICP method. The weight composition of constituent elements was determined: Mn 25%, Fe 65.34%, and Zn 9.66%; so the molecular formula of the shell was calculated: $Mn_{0.77}Zn_{0.25}Fe_{1.98}O_4$. In the next step, the core/shell adsorbent was analyzed by ICP method. The weight composition of its constituents was determined: Mn 12.56%, Fe 82.59%, and Zn 4.85%. So, the chemical formula of the core/shell adsorbent was calculated $Fe_3O_4/Mn_{0.77}Zn_{0.25}Fe_{1.98}O_4$.

The XRD powder diffraction pattern of the Fe_3O_4 magnetic nanoparticles (core) are shown in Fig. 4. The peaks

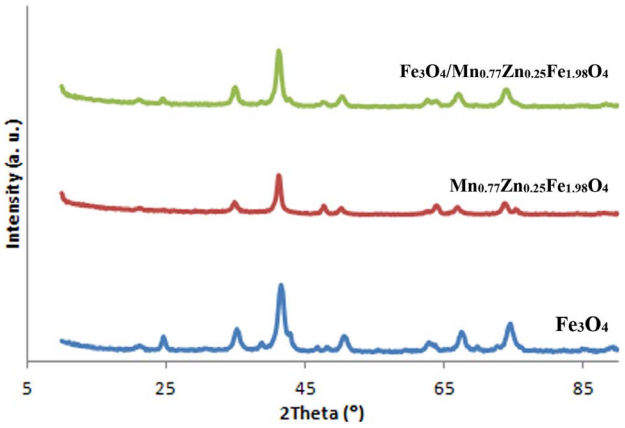

Fig. 4. XRD pattern of Fe_3O_4 (core), $Mn_{0.77}Zn_{0.25}Fe_{1.98}O_4$ (shell), and $Fe_3O_4/Mn_{0.77}Zn_{0.25}Fe_{1.98}O_4$ (core/shell) magnetic nanoparticles.

at 21.89°, 41.57°, 50.81°, 63.29°, 67.49°, and 74.57° are characteristic of Fe_3O_4 (JCPDS File No. 11-0614). The peaks observed at 24.77°, 46.85°, and 48.17° belong to FeO(OH) (JCPDS File No. 29-0713). The XRD pattern of $Mn_{0.77}Zn_{0.25}Fe_{1.98}O_4$ (shell) shows peaks at 34.97°, 41.21°, 50.33°, and 63.89° which belong to Franklinite maganoan (Zinc Manganese Iron oxide) (JCPDS File No. 01-087-1171). The other peaks are also recognized: peaks at 47.69° to δ-$(Fe_{0.6}Mn_{0.33})$OOH, FeO(OH), Fe_2O_3, and peaks at 73.61° and 75.29° can be attributed to FeO(OH) and Fe_2O_3, respectively. The XRD pattern of $Fe_3O_4/Mn_{0.77}Zn_{0.25}Fe_{1.98}O_4$ (core/shell sample) shows peaks at 21.05°, 34.97°, 41.33°, 50.33°, and 74.09° indicating the existence of Fe_3O_4 (JCPDS File No. 11-0614) and Franklinite structure of the shell (JCPDS No. 01-087-1171). The other peaks are detected at 25.13° to FeO(OH), 62.93° to Franklinite, and 67.01° to Fe_3O_4 can be attributed.

The average crystallite sizes of the nanoparticles were calculated based on the peak of 41° using Scherrer's equation as follows [34]:

$$D = \frac{K\lambda}{\beta\cos\theta} \tag{4}$$

where D is the mean dimension of the crystalline, K is a constant (K = 0.9), β is the peak full width at half of the maximum height, and θ is the Bragg diffraction angle.

The crystalline sizes of Fe_3O_4, $Mn_{0.77}Zn_{0.25}Fe_{1.98}O_4$, and $Fe_3O_4/Mn_{0.77}Zn_{0.25}Fe_{1.98}O_4$ were calculated as 11.32, 22.54, and 31.77 nm, respectively. It is obvious that coating Fe_3O_4 by $Mn_{0.77}Zn_{0.25}Fe_{1.98}O_4$ increased the crystalline sizes from 11.32 to 31.77 nm.

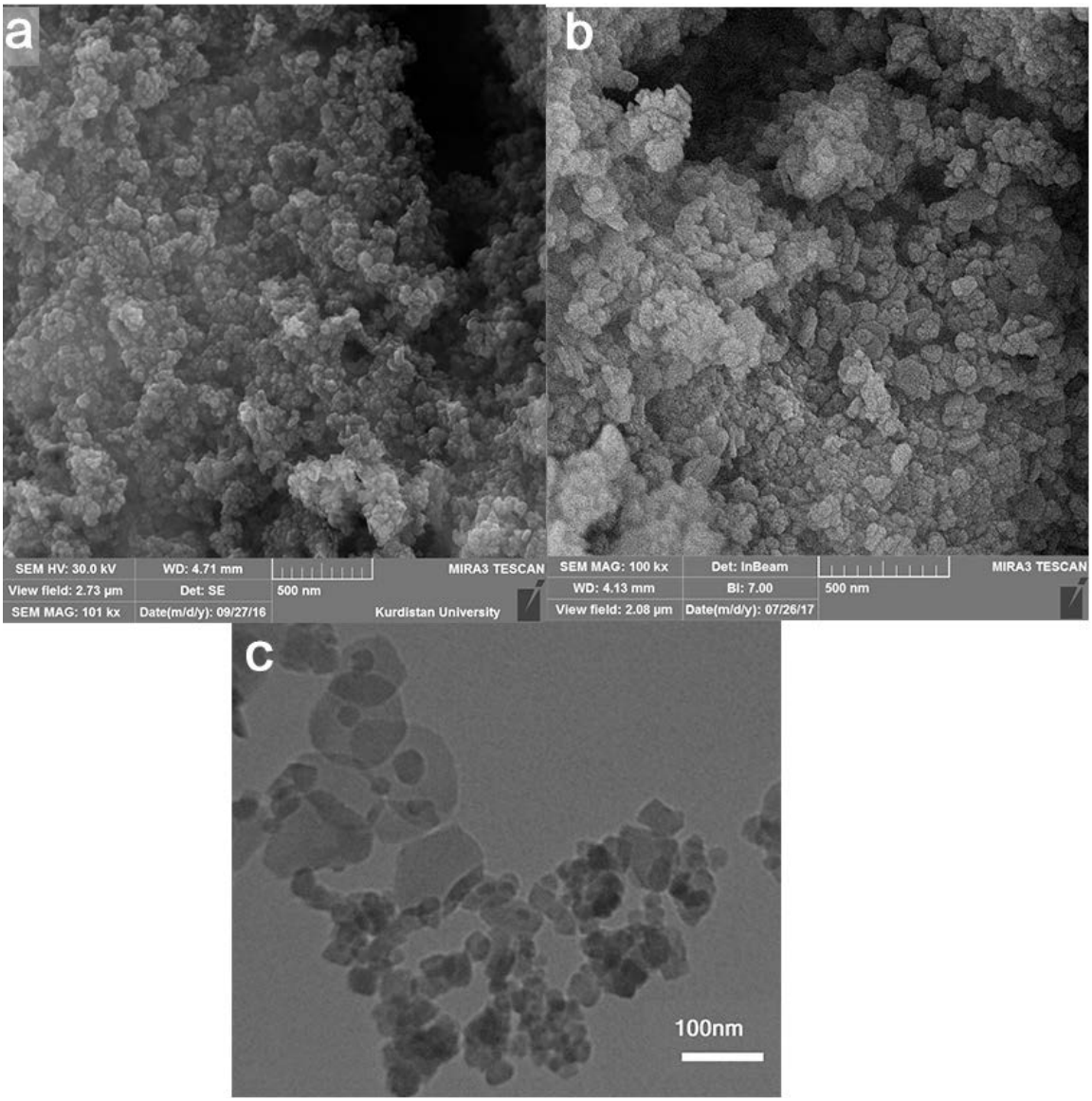

Fig. 5. (a) SEM image of Fe_3O_4; (b) SEM image of $Fe_3O_4/Mn_{0.77}Zn_{0.25}Fe_{1.98}O_4$; (c) TEM image of $Fe_3O_4/Mn_{0.77}Zn_{0.25}Fe_{1.98}O_4$.

Figs. 5(a) and (b) show the SEM images of Fe_3O_4 and $Fe_3O_4/Mn_{0.77}Zn_{0.25}Fe_{1.98}O_4$. It is obvious that the shapes of grains have a sphere-like shape. $Fe_3O_4/Mn_{0.77}Zn_{0.25}Fe_{1.98}O_4$ grains are larger than Fe_3O_4 due to the thickness of the shell layer. TEM image of Fig. 5(c) shows that Fe_3O_4 nanoparticles are embedded in the shell layer. The magnetic particles agglomerated because of magnetic dipole interactions.

XPS spectra of the core/shell sample are shown in Fig. 6. Peaks with binding energies of 710.88, 718.78, 724.48, and 733.08 eV are attributed to the Fe 2p 3/2, satellite 2p 3/2, 2p 1/2, and satellite 2p 1/2; respectively (Fig. 6(a)). These peaks confirm the existence of Fe^{3+} in the surface of the sample (shell) [35,36]. Fig. 6(b) shows two peaks at 641.68 and 653.18 eV which can be assigned to Mn 2p 3/2 and Mn 2p 1/2, respectively, and indicates the existence of Mn^{4+} [36,37]. Fig. 6(c) shows peaks with the binding energies of 1,021.38 and 1,044.48 eV which are attributed to Zn 2p 3/2 and 2p 1/2, respectively, and confirm the existence of Zn^{2+} in the surface of the adsorbent [38,39].

The magnetic properties (VSM) of the Fe_3O_4, $Mn_{0.77}Zn_{0.25}Fe_{1.98}O_4$, and $Fe_3O_4/Mn_{0.77}Zn_{0.25}Fe_{1.98}O_4$ are shown in Fig. 7. No hysteresis loop was observed; so the samples are superparamagnetic. The saturation magnetism (M_s), and coercive force (H_c) for Fe_3O_4 are: 60 emus/g and 5.5 Oe, respectively. They are 60.59 emu/g and 8 Oe for $Mn_{0.77}Zn_{0.25}Fe_{1.98}O_4$, respectively; and for $Fe_3O_4/Mn_{0.77}Zn_{0.25}Fe_{1.98}O_4$, they are 105.39 emu/g and 8 Oe, respectively. The magnetic saturation of the $Fe_3O_4/Mn_{0.77}Zn_{0.25}Fe_{1.98}O_4$ is larger than Fe_3O_4 and $Mn_{0.77}Zn_{0.25}Fe_{1.98}O_4$ due to the addition of the magnetic property of the core (Fe_3O_4) and shell ($Mn_{0.77}Zn_{0.25}Fe_{1.98}O_4$) in the core/shell nanoparticles [26].

Phosphate adsorption experiments were done in the pH range of 2–8, and its results are shown in Fig. 8. The results show that phosphate adsorption decreased when pH increased. In the pH range of 3–7, $H_2PO_4^-$ is the dominant specie of the phosphate anions. In this pH range, the surface of the $Fe_3O_4/Mn_{0.77}Zn_{0.25}Fe_{1.98}O_4$ was protonated and

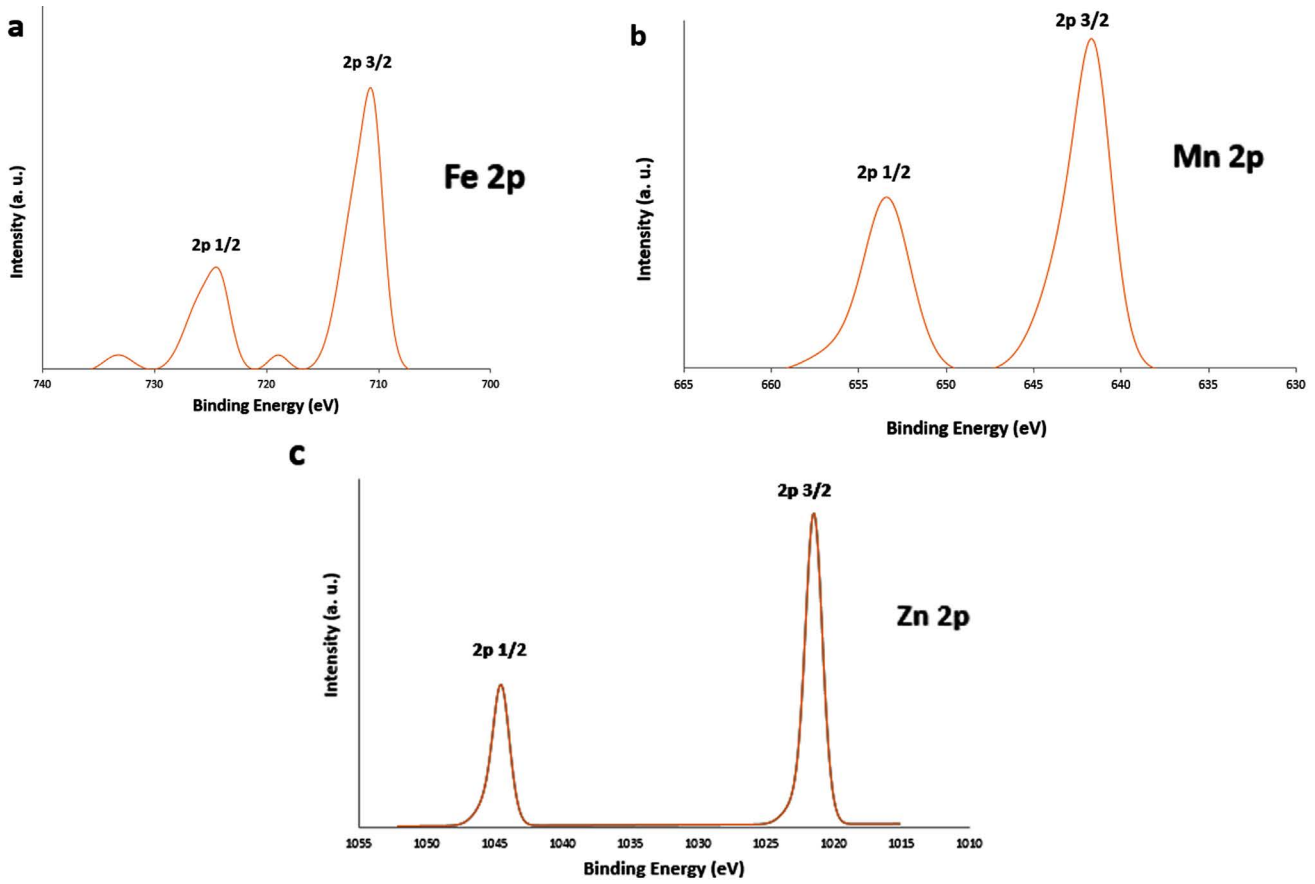

Fig. 6. XPS spectra of the core/shell sample (a) Fe 2p; (b) Mn 2p; (c) Zn 2p.

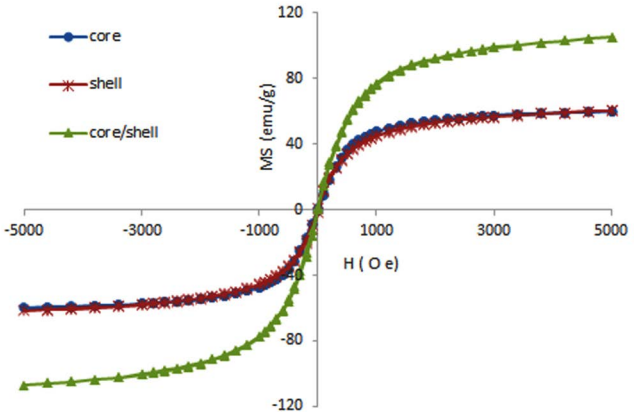

Fig. 7. Magnetic hysteresis of Fe_3O_4, $Mn_{0.77}Zn_{0.25}Fe_{1.98}O_4$, and $Fe_3O_4/Mn_{0.77}Zn_{0.25}Fe_{1.98}O_4$ nanoparticles.

became positively charged, and can strongly adsorb negative phosphate anions $H_2PO_4^-$ due to attractive electrostatic forces between opposite charges. In high pH, the $Fe_3O_4/Mn_{0.77}Zn_{0.25}Fe_{1.98}O_4$ adsorbent was deprotonated and negatively charged. The repulsive electrostatic forces between negatively charged adsorbent and HPO_4^{2-} phosphate anions caused decrease in phosphate removal yield. In high pH, competition between OH^- and HPO_4^{2-} groups also decreased phosphate adsorption. Fig. 8 shows that phosphate removal was completed and reached to 99.77% at pH 2 [9].

3.5. Adsorption model

The adsorption isotherm model contributes to understanding of the adsorbate–adsorbent interactions. Langmuir and Freundlich are the most common adsorption models. The linear form of Langmuir is as follows [40]:

$$\frac{C_e}{q_e} = \frac{C_e}{q_m} + \frac{1}{K_L q_m} \tag{5}$$

where q_e (mg/L) is the equilibrium adsorption capacity, C_e (mg/L) is the equilibrium concentration of phosphate solution, q_m (mg/g) is the maximum adsorption capacity, and K_L (L/mg) is the Langmuir constant. The linear form of Freundlich model is as follows [40]:

$$\log q_e = \log K_F + \frac{1}{n}\log C_e \tag{6}$$

where q_e (mg/L) is the phosphate equilibrium adsorption capacity, C_e (mg/L) is the concentration of phosphate solution at equilibrium, K_F ($mg^{1-1/n}L^{1/n}/g$) and n are constants related to the adsorption capacity.

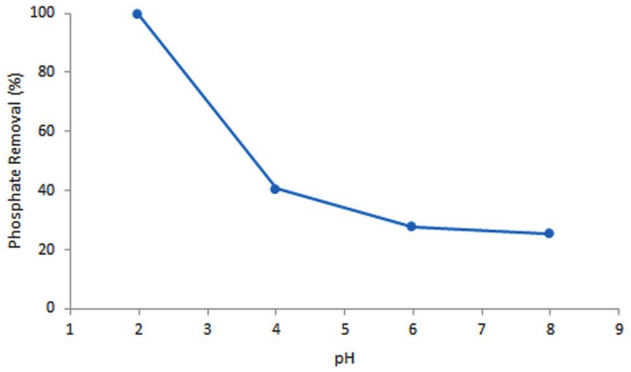

Fig. 8. Effect of pH on phosphate adsorption; operating conditions: initial phosphate concentration 80 mg/L, adsorbent dose 5 g/L, time 2 h.

Figs. 9(a) and (b) show the linear forms of the Langmuir and Freundlich isotherm models for phosphate removal by $Fe_3O_4/Mn_{0.77}Zn_{0.25}Fe_{1.98}O_4$. The results of data fitting are shown in Table 5. The larger R^2 shows the data fit better to the Langmuir isotherm.

In Table 6, the maximum adsorption capacity of the $Fe_3O_4/Mn_{0.77}Zn_{0.25}Fe_{1.98}O_4$ is compared with other adsorbents. The maximum adsorption capacity for phosphate removal 30.77 mg/g is reported which is as large as others (Table 6). In addition, the nanomagnetic core/shell adsorbent $Fe_3O_4/Mn_{0.77}Zn_{0.25}Fe_{1.98}O_4$ has the advantage of easy separation from water by an external magnetic force.

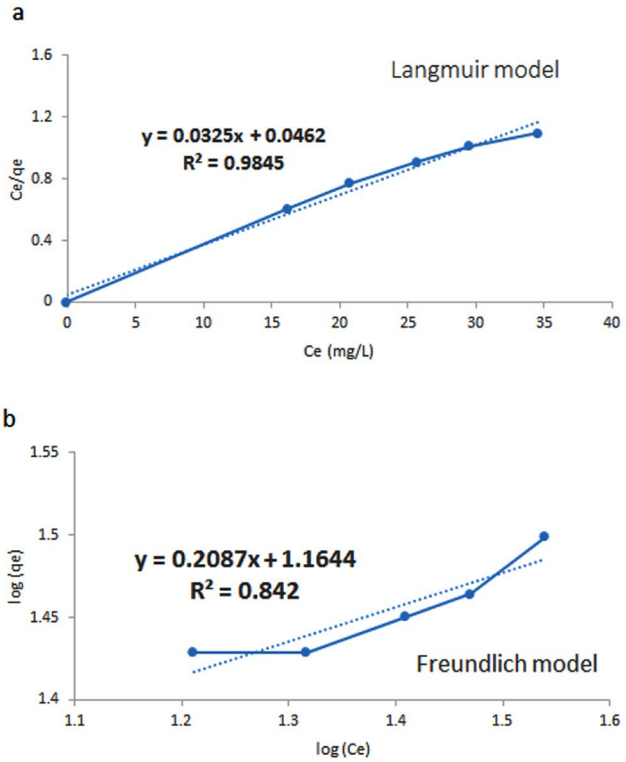

Fig. 9. Adsorption isotherm of phosphate by $Fe_3O_4/Mn_{0.77}Zn_{0.25}Fe_{1.98}O_4$ (a) Langmuir model; (b) Freundlich model.

3.6. Adsorption and regeneration studies

Furthermore, regeneration experiments for $Fe_3O_4/Mn_{0.77}Zn_{0.25}Fe_{1.98}O_4$ were done. In the adsorption step, 5 g/L of adsorbent, and 200 mL of phosphate with the initial concentration of 87.5 mg/L and pH 4 were mixed for 3 h. After adsorption, in the regeneration step, the adsorbent was regenerated by 40 mL of NaOH (0.1 mol/L) for 4 h. After adsorption/desorption operation, the regenerated adsorbent was washed by deionized water until pH reached neutral. Then, the adsorbent was filtered, dried, and used in the next cycle. After first adsorption cycle, the phosphate removal was 85%, in the second, third, fourth, and fifth cycle; the adsorption removals were 82.82%, 73.6%, 68.6%, and 65.1%; respectively. The phosphate adsorption decreased in consecutive operation (Fig. S1).

Table 5
Langmuir and Freundlich constants and correlation coefficients for phosphate adsorption by $Fe_3O_4/Mn_{0.77}Zn_{0.25}Fe_{1.98}O_4$

Adsorbate	Langmuir			Freundlich		
	q_m (mg/g)	K_L (L/mg)	R^2	K_F ($mg^{1-1/n}L^{1/n}/g$)	n	R^2
Phosphate	30.77	0.7034	0.9845	14.60	4.79	0.8420

Table 6
Comparison between different adsorbents for the removal of phosphate

Adsorbent	pH	T (°C)	q_m (mg/g)	Reference
Fe-Ti bimetal oxide	6.8	20	35.4	[8]
Magnetic iron oxide	2	30	3.06	[23]
$CuFe_2O_4$	2.64	45	13.8	[6]
Magnetic Fe-Zr binary oxide	4	25	13.65	[22]
Fe_3O_4@mZrO_2	7	25	39.1	[41]
Fe-Mn binary oxide	5.6	25	33.2	[21]
$Fe_3O_4/Mn_{0.77}Zn_{0.25}Fe_{1.98}O_4$	3	25	30.77	This work

4. Conclusions

Core/shell magnetic nanoparticles of $Fe_3O_4/Mn_{0.77}Zn_{0.25}Fe_{1.98}O_4$ were synthesized by coprecipitation method and used as adsorbent for removal of phosphate from water. The core/shell adsorbent composition is a function of the shell constituent solutions and the mass of the Fe_3O_4 (core) nanoparticles. The RSM and D-optimal methods were used to define experiments to determine the adsorbent composition with the highest phosphate removal. The iron content in relation to the Zn and Mn was always adjusted in such a way that an iron spinel structure would be obtained. The mathematical empirical model was developed using experimental data and Design Expert software (version 7). The empirical model showed a good correlation to the experiments. The independent variables, that is, Fe_3O_4 mass and concentrations of Mn^{2+} and Zn^{2+}solutions had significant effects on the phosphate adsorption. Interactions between independent variables also had effects on the response.

One of the optimum points suggested by the software was selected. Concentration of Mn^{2+} solution 0.6 mol/L, Zn^{2+} 0.49 mol/L, Fe^{3+} 1.91 mol/L, and Fe_3O_4 mass 2.17 g were applied to synthesize the adsorbent. ICP determined the composition of the selected adsorbent $Fe_3O_4/Mn_{0.77}Zn_{0.25}Fe_{1.98}O_4$. The XRD results indicated the Franklinite structure of the shell. TEM and SEM results analysis confirmed the adsorbent core/shell structure. Decrease in the pH of the phosphate solution increased adsorption. Maximum phosphate adsorption capacity was 30.77 mg/g which was comparable with others reported in the literature. The experimental data corresponded better to the Langmuir adsorption model. The results of this work showed that suitable selection of the shell constituent solutions concentrations and Fe_3O_4 mass lead to a magnetic core/shell adsorbent which can be separated easily from the solution with an external magnet and have a good yield for phosphate adsorption from water.

Acknowledgment

The financial support of the University of Kurdistan is greatly acknowledged.

References

[1] G. Li, S. Gao, G. Zhang, X. Zhang, Enhanced adsorption of phosphate from aqueous solution by nanostructured iron(III)–copper(II) binary oxides, Chem. Eng. J., 235 (2014) 124–131.
[2] Y. Li, Q. Xie, Q. Hu, C. Li, Z. Huang, X. Yang, H. Guo, Surface modification of hollow magnetic Fe_3O_4@NH_2-MIL-101(Fe) derived from metal-organic frameworks for enhanced selective removal of phosphates from aqueous solution, Sci. Rep., 6 (2016) 30651–30662.
[3] N. Mehrabi, M. Soleimani, H. Sharififard, M. Madadi Yeganeh, Optimization of phosphate removal from drinking water with activated carbon using response surface methodology (RSM), Desal. Wat. Treat., 57 (2016) 15613–15618.
[4] M. Arshadi, J. Etemad Gholtash, H. Zandi, S. Foroughifard, Phosphate removal by a nano-biosorbent from the synthetic and real (Persian Gulf) water samples, RSC. Adv., 5 (2015) 43290–43302.
[5] A. Alshameri, C. Yan, X. Lei, Enhancement of phosphate removal from water by TiO_2/Yemeni natural zeolite: preparation, characterization and thermodynamic, Microporous Mesoporous Mater., 196 (2014) 145–157.
[6] Y.-J. Tu, C.-F. You, Phosphorus adsorption onto green synthesized nano-bimetal ferrites: equilibrium, kinetic and thermodynamic investigation, Chem. Eng. J., 251 (2014) 285–292.
[7] A.F. de Sousa, T.P. Braga, E.C.C. Gomes, A. Valentini, E. Longhinotti, Adsorption of phosphate using mesoporous spheres containing iron and aluminum oxide, Chem. Eng. J., 210 (2012) 143–149.
[8] J. Lu, D. Liu, J. Hao, G. Zhang, B. Lu, Phosphate removal from aqueous solutions by a nano-structured Fe–Ti bimetal oxide sorbent, Chem. Eng. Res. Des., 93 (2015) 652–661.
[9] L. Yan, K. Yang, R. Shan, T. Yan, J. Wei, S. Yu, H. Yu, B. Du, Kinetic, isotherm and thermodynamic investigations of phosphate adsorption onto core–shell Fe_3O_4@LDHs composites with easy magnetic separation assistance, J. Colloid Interface Sci., 448 (2015) 508–516.
[10] H. Jiang, P. Chen, S. Luo, X. Tu, Q. Cao, M. Shu, Synthesis of novel nanocomposite Fe_3O_4/ZrO_2/chitosan and its application for removal of nitrate and phosphate, Appl. Surf. Sci., 284 (2013) 942–949.
[11] E.M. van Voorthuizen, A. Zwijnenburg, M. Wessling, Nutrient removal by NF and RO membranes in a decentralized sanitation system, Water Res., 39 (2005) 3657–3667.
[12] https://www.sswm.info/content/membrane-filtration (accessed 27 January 2018).
[13] M. Arshadi, A.R. Faraji, M. Mehravar, Dye removal from aqueous solution by cobalt-nano particles decorated aluminum silicate: kinetic, thermodynamic and mechanism studies, J. Colloid Interface Sci., 440 (2015) 91–101.
[14] L. Filipponi, D. Sutherland, Nanotechnologies: Principles, Applications, Implications and Hands-Activities, European Commission, Luxembourg, 2013.
[15] L. Cui, L. Hu, X. Guo, Y. Zhang, Y. Wang, Q. Wei, B. Du, Kinetic, isotherm and thermodynamic investigations of Cu^{2+} adsorption onto magnesium hydroxyapatite/ferroferric oxide nanocomposites with easy magnetic separation assistance, J. Mol. Liq., 198 (2014) 157–163.
[16] A.Z.M. Badruddoza, A.S.H. Tay, P.Y. Tan, K. Hidajat, M.S. Uddin, Carboxymethyl-β-cyclodextrin conjugated magnetic nanoparticles as nano-adsorbents for removal of copper ions: synthesis and adsorption studies, J. Hazard. Mater., 185 (2011) 1177–1186.
[17] R. Davarnejad, P. panahi, Cu (II) removal from aqueous wastewaters by adsorption on the modified Henna with Fe_3O_4 nanoparticles using response surface methodology, Sep. Purif. Technol., 158 (2016) 286–292.
[18] M.A. Zulfikar, S. Afrita, D. Wahyuningrum, M. Ledyastuti, Preparation of Fe_3O_4-chitosan hybrid nano-particles used for humic acid adsorption, Environ. Nanotechnol. Monit. Manage., 6 (2016) 64–75.
[19] J. Yang, Q. Zeng, L. Peng, M. Lei, H. Song, B. Tie, J. Gu, La EDTA coated Fe_3O_4 nanomaterial: Preparation and application in removal of phosphate from water, J. Environ. Sci., 25 (2013) 413–418.
[20] Q. Gao, F. Chen, J. Zhang, G. Hong, J. Ni, X. Wei, D. Wang, The study of novel Fe_3O_4@γ-Fe_2O_3 core/shell nanomaterials with improved properties, J. Magn. Magn. Mater., 321 (2009) 1052–1057.
[21] G. Zhang, H. Liu, R. Liu, J. Qu, Removal of phosphate from water by a Fe–Mn binary oxide adsorbent, J. Colloid Interface Sci., 335 (2009) 168–174.
[22] F. Long, J.L. Gong, G.M. Zeng, L. Chen, X.Y. Wang, J.H. Deng, Q.Y. Niu, H.Y. Zhang, X.R. Zhang, Removal of phosphate from aqueous solution by magnetic Fe–Zr binary oxide, Chem. Eng. J., 171 (2011) 448–455.
[23] S.-Y. Yoon, C.-G. Lee, J.-A. Park, J.-H. Kim, S.-B. Kim, S.-H. Lee, J.-W. Choi, Kinetic, equilibrium and thermodynamic studies for phosphate adsorption to magnetic iron oxide nanoparticles, Chem. Eng. J., 236 (2014) 341–347.
[24] L. Lai, Q. Xie, L. Chi, W. Gu, D. Wu, Adsorption of phosphate from water by easily separable Fe_3O_4@SiO_2 core/shell magnetic nanoparticles functionalized with hydrous lanthanum oxide, J. Colloid Interface Sci., 465 (2016) 76–82.
[25] R.Y. Hong, S.Z. Zhang, G.Q. Di, H.Z. Li, Y. Zheng, J. Ding, D.G. Wei, Preparation, characterization and application of

Fe_3O_4/ZnO core/shell magnetic nanoparticles, Mater. Res. Bull., 43 (2008) 2457–2468.
[26] R.Y. Hong, J.H. Li, X. Cao, S.Z. Zhang, G.Q. Di, H.Z. Li, D.G. Wei, On the $Fe_3O_4/Mn_{1-x}Zn_xFe_2O_4$ core/shell magnetic nanoparticles, J. Alloys Compd., 480 (2009) 947–953.
[27] R.P. Kralchevska, R. Prucek, J. Kolařík, J. Tuček, L. Machala, J. Filip, V.K. Sharma, R. Zbořil, Remarkable efficiency of phosphate removal: ferrate(VI)-induced in situ sorption on core-shell nanoparticles, Water Res., 103 (2016) 83–91.
[28] L.S. Clesceri, A.E. Greenberg, A.D. Eaton, Standard Methods for the Examination of Water and Wastewater, 20th ed., American Public Health Association, 1999.
[29] D.C. Montgomery, Design and Analysis of Experiments, fifth ed., John Wiley & Sons, New York, 2001.
[30] http://www.itl.nist.gov/div898/handbook/ (accessed 27 January 2018).
[31] C. Wang, S. Yang, H. Chang, Y. Peng, J. Li, Structural effects of iron spinel oxides doped with Mn, Co, Ni and Zn on selective catalytic reduction of NO with NH_3, J. Mol. Catal. A: Chem., 376 (2013) 13–21.
[32] S. Rajesh, S. Rajakarunakaran, R. Sudhakara Pandian, Modeling and optimization of Sliding specific wear and coefficient of friction of aluminum based red mud metal matrix composite using Taguchi method and response surface methodology, Mater. Phys. Mech., 15 (2012) 150–166.
[33] M. Feilizadeh, M. Rahimi, S.M. Esmaeil Zakeri, N. Mahinpey, M. Vossoughi, M. Qanbarzadeh, Individual and interaction effects of operating parameters on the photocatalytic degradation under visible light illumination: response surface methodological approach, Can. J. Chem. Eng., 95 (2017) 1228–1235.
[34] S.H. Kareem, A.A. Ati, M. Shamsuddin, S.L. Lee, Nanostructural, morphological and magnetic studies of PEG/$Mn_{(1-x)}Zn_{(x)}Fe_2O_4$ nanoparticles synthesized by co-precipitation, Ceram. Int., 41 (2015) 11702–11709.
[35] H. Yang, Q. Liu, S. Masse, H. Zhang, L. Li, T. Goradin, Hierarchically-organized, well-dispersed hydroxyapatite-coated magnetic carbon with combined organics and inorganics removal properties, Chem. Eng. J., 275 (2015) 152–159.
[36] S. Xing, Z. Zhou, Z. Ma, Y. Wu, Characterization and reactivity of $Fe_3O_4/FeMnO_x$ core/shell nanoparticles for methylene blue discoloration with H_2O_2, Appl. Catal., B, 107 (2011) 386–392.
[37] L. Liu, X. Zhang, R. Wang, J. Liu, Facile synthesis of Mn_2O_3 hollow and core–shell cube-like nanostructures and their catalytic properties, Superlattices Microstruct., 72 (2014) 219–229.
[38] I.G. Morozov, O.V. Belousova, D. Ortega, M.K. Mafina, M.V. Kuzntcov, Structural, optical, XPS and magnetic properties of Zn particles capped by ZnO nanoparticles, J. Alloys Compd., 633 (2015) 237–245.
[39] Z.-W. Wu, S.-L. Tyan, H.-H. Chen, J.-C.-A. Huang, Y.-C. Huang, C.-R. Lee, T.-S. Mo, Temperature-dependent photoluminescence and XPS study of ZnO nanowires grown on flexible Zn foil via thermal oxidation, Superlattices Microstruct., 107 (2017) 38–43.
[40] F. Zhuang, R. Tan, W. Shen, X. Zhang, W. Xu, W. Song, Monodisperse magnetic hydroxyapatite/Fe_3O_4 microspheres for removal of lead(II) from aqueous solution, J. Alloys Compd., 637 (2015) 531–537.
[41] A. Sarkar, S. Kanti Biswas, P. Pramanik, Design of a new nanostructure comprising Mesoporous ZrO_2 shell and magnetite core (Fe_3O_4@mZrO_2) and study of its phosphate ion separation efficiency, J. Mater. Chem., 20 (2010) 4417–4424.

Supplementary information

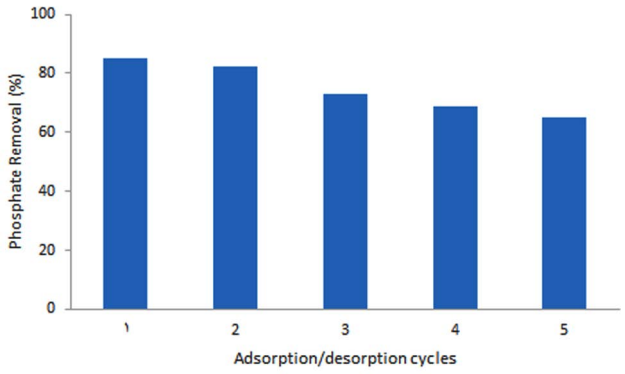

Fig. S1. Effect of the regeneration cycles on phosphate adsorption.